Ramjan Ali, Iftekhar Anam, Shigeo Yoshida
Structure and Environment 2023, vol. 15, (4), pp. 208-216, Article number: el 018
https://doi.org/10.30540/sae-2023-018

Structure and Environment
ISSN 2081-1500
e-ISSN 2657-6902
https://content.sciendo.com/sae
https://sae.tu.kielce.pl

sciendo

Kielce University of Technology

DOI: 10.30540/sae-2023-018

CFD AND EXPERIMENTAL INVESTIGATION OF THE IMPACT OF DIMENSIONAL MODIFICATIONS ON WIND PRESSURE COEFFICIENT DISTRIBUTION

ANALIZA CFD ORAZ METODY EKSPERYMENTALNE W BADANIACH WPŁYWU MODYFIKACJI WYMIARÓW NA ROZKŁAD WSPÓŁCZYNNIKA PARCIA WIATRU

RAMJAN ALI*
European University of Bangladesh, Bangladesh
IFTEKHAR ANAM
University of Asia Pacific, Bangladesh
SHIGEO YOSHIDA
Kyushu University, Japan

Abstract

The sway of tall buildings in the wind is a fascinating and crucial consideration for professionals in the structural, environmental, and architectural fields. Previous research has related wind pressure to building load and natural ventilation, but few studies have looked at how building dimensions impact wind pressure. This study examined wind pressure coefficient distributions within and around several rectangular-shaped high-rise buildings using experimental and computational fluid dynamics approaches. The height-to-width ratio and height-to-thickness (length) ratio significantly affected the wind characteristics of buildings. The windward side with a narrower width experienced higher wind pressure, while the larger leeward side experienced a more negative wind effect. Wind pressure coefficient distribution varies with decrease in the side ratio. However, the side ratio of the building had little influence on positive wind pressure at wind incidence angle of 0°, which was a surprising finding. Pressure coefficients were evaluated and compared with standards by measuring fluctuating wind pressures at pressure points on all surfaces of models, and then calculating the mean, maximum, minimum, and r.m.s. values of these coefficients.

Keywords: Computational Fluid Dynamics, Wind pressure coefficient, Building dimensions, Windward, Leeward, Side Ratio

Streszczenie

Kołysanie się wysokich budynków pod wpływem wiatru jest fascynującym i kluczowym zagadnieniem dla specjalistów w dziedzinie konstrukcji, ochrony środowiska i architektury. W niniejszym artykule zbadano rozkłady współczynnika parcia wiatru wewnątrz i wokół kilku budynków wysokich o kształcie prostokąta, stosując metody eksperymentalne i numeryczne (obliczeniowa dynamika płynów). Stosunek wysokości budynku do jego szerokości oraz stosunek wysokości budynku do jego grubości (długości) miały znaczący wpływ na charakterystykę oddziaływania wiatru. Większe ciśnienie wiatru odnotowano po stronie nawietrznej o mniejszej szerokości, podczas gdy na większej ścianie od strony zawietrznej

*Corresponding Author: e-mail: ramjanali.ce@outlook.com

oddziaływanie wiatru było bardziej negatywne. Rozkład współczynnika parcia wiatru zmienia się wraz ze spadkiem stosunku boków. Jednak stosunek ten miał niewielki wpływ na dodatnie ciśnienie wiatru przy kierunku wiatru 0°, co było zaskakującym odkryciem. Współczynniki ciśnienia zostały ocenione i porównane z podejściem normowym poprzez pomiar zmiennego ciśnienia wiatru w punktach parcia na wszystkich powierzchniach modeli, a następnie obliczenie średnich, maksymalnych, minimalnych i średnich kwadratowych wartości tych współczynników.

Słowa kluczowe: obliczeniowa dynamika płynów, współczynnik ciśnienia wiatru, strona nawietrzna, strona zawietrzna, proporcje boków

1. INTRODUCTION

In building science, wind impacts are directly linked to building loads and natural ventilation. Building designs, wind features, and site factors contribute to the complex and changeable nature of air flows around structures, as established by various studies (Blocken, 2014). Despite differences in parameter values between international wind regulations and codes, regression methods such as the logarithmic law, exponential law, and modified logarithmic law have been used to develop wind profiles (Kwon & Kareem, 2013). These profiles play an essential part in turbulence models and the use of computational fluid dynamics (CFD) methods, determining the dependability of numerical simulations. Scholars have deployed simulations to examine the usefulness of turbulent models, including extensive eddy simulation and the conventional k- turbulent model, demonstrating strong agreement with experimental results (Murakami & Mochida, 1988; Murakami, Mochida, & Hibi, 1987). However, the latter strategy proved superior in capturing unstable fields. Wind velocity, as well as pressure variations within and around structures, have been comprehensively explored using various k- models, enabling substantial progress in understanding wind features (Baskaran & Stathopoulos, 1989, 1993; Stathopoulos & Baskaran, 1996). Designing lateral systems and claddings for high-rise structures involves careful consideration of wind-induced vibrations. Standards such as ASCE Standard No. 7-05, Bangladesh National Building Code (2020), and Standards Australia/Standards New Zealand (2011) give instructions for analyzing wind force coefficients as well as wind pressure coefficients (Kwon & Kareem, 2013). While these rules include coefficients for rectangular and square structures with varying aspect ratios and heights at defined wind exposure angles, they lack suggestions for greatly expanded rectangular plan-shaped buildings or oblique wind incidence angles. Extensive research has been conducted on the wind pressure distributions of rectangular models, focusing on factors such as side ratios, boundary layer conditions, and wind orientations. Kareem and Cermak (1984) conducted studies to examine the pressure distribution along the sidewalls of square models under various boundary layer flow conditions. In a complementary study, Kareem (1990) investigated the influence of turbulent boundary layer flows on the temporal and spatial characteristics of pressure fields observed on the surfaces of prismatic structures. In wind tunnel experiments conducted on an 11-story building, Jóźwiak et al. (1995) observed that on the sheltered side, specifically in the area between buildings, there were significantly higher negative pressures compared to those recorded for a stand-alone building, reaching up to 1.8 times the magnitude. However, the interference effect diminishes greatly when the building is strategically positioned. Additionally, Saathoff and Melbourne (1989) employed rectangular prisms and extended plates that were flat with square edge shapes to acquire insights into specific components of the two-dimensional detachment and restoration process, as well as the development of maximal suction forces. Investigations by Miyata and Miyazaki (1980), Lee (1975), and Vickery (1966) involved the measurement of the surface forces and relationships between dimensions in a 2-dimensional flow. According to Lee's study, an increase in perpendicular turbulence around the cube led to a decrease in base pressure and a reversal of pressure on the side faces. To examine how side ratios and wind direction affect the distribution of wind pressure, this research integrates experimental investigation with computational fluid dynamics (CFD) analysis.

2. NUMERICAL MODEL VALIDATION

The present study selected the model of the Commonwealth Advisory Aeronautical Council (CAARC) building for the numerical model validation. The CAARC model is shaped like a rectangular prism and measures 100 feet (x), 150 feet (y), and 600 feet (z) in height, as shown in Figure 1. The current study employed a wind velocity profile for an open exposure, the power low exponent of which was 0.16, which could be seen in Figure 2. A system of Cartesian

coordinates (x, y, z) was used to represent the flow, the x-axis represents the direction of the stream, the y-axis is stacked vertically, and the z-axis is in the opposite direction of the stream. Information about the CFD mesh is as follows: (1) mesh density 35%, (2) number of mesh 1871820, and (3) minimum grid size 1.37 feet.

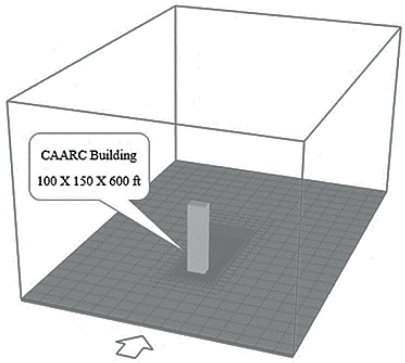

Fig. 1. Computational wind tunnel setup

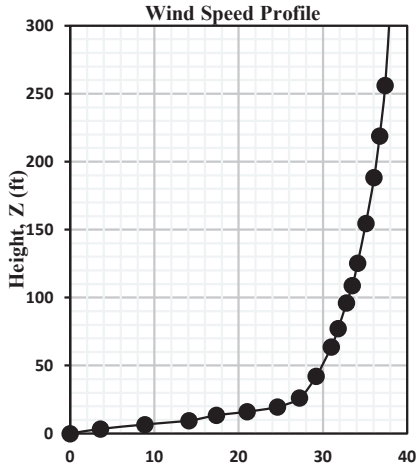

Fig. 2. Wind Speed Profile (Dagnew et al. 2009)

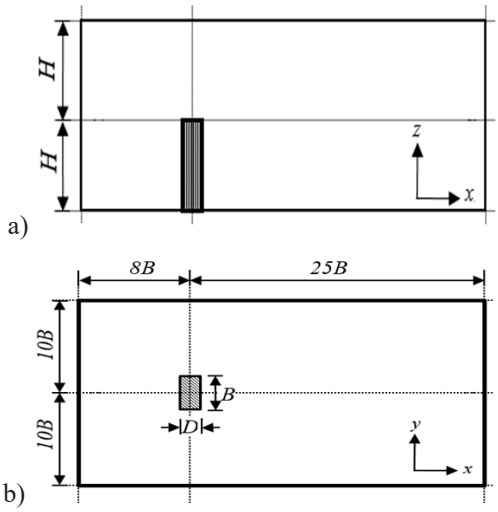

Fig. 3. Side (a) and top (b) view of the boundary conditions and computational domain

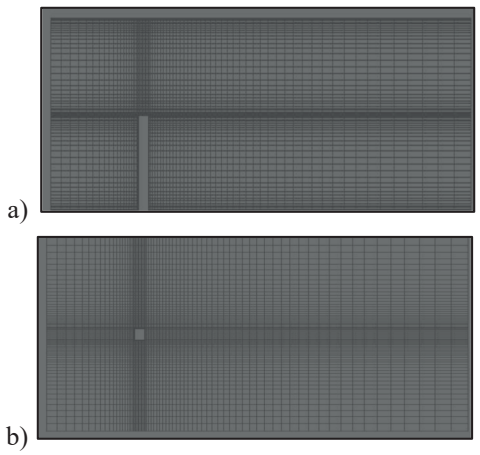

Fig. 4. Side (a) and top (b) view of the typical grid used for the study

The FLUENT code provides four choices for Subgrid-Scale (SGS) approach for LES. These are: Smagorinsky–Lilly model, Dynamic Smagorinsky–Lilly model, Wall-adapting local eddy-viscosity model, and Dynamic SGS kinetic energy model. The dynamic SGS kinetic energy model is used in this study as it accounts for the transport of the SGS turbulence kinetic energy, which was found to be better than an algebraic expression based on local equilibrium assumptions given by the Smagorinsky series. The Smagorinsky series assumes that equilibrium exists between the transferred energy through the grid-filter scale and the dissipation of kinetic energy at small subgrid scales. However, for high Reynolds number bluff body flows, the local equilibrium assumption is questionable. The SGS kinetic energy of the dynamic SGS kinetic energy model is defined as $Ksgs = \frac{1}{2}\left(\overline{U_k^2} - \overline{U_k^2}\right)$ which is obtained by contracting the subgrid-scale stress in $\tau_{ij} = \rho\overline{U_i U_j} - \rho\overline{U_i}\,\overline{U}$. The SGS eddy viscosity, μ_t, is computed using $Ksgs$ as, $\mu_t = CkKsgs^{1/2}\Delta f$, where Δf is the filter size computed from $\Delta f = v^{1/3}$. The subgrid-scale stress can then be written as $\tau_{ij} \quad \frac{2}{3}ksgs\delta_{i,j} \quad 2\mu_t\overline{S}_{i,j}$, while $Ksgs$ is obtained by solving its transport equation:

$$\frac{\partial ksgs}{\partial_t} + \frac{\partial \overline{U_j}.ksgs}{\partial x_j} =$$

$$-\tau_{ij}\frac{\partial \overline{U_j}}{\partial x_j} - C_\varepsilon \frac{Ksgs^{\frac{2}{3}}}{\Delta f} + \frac{\partial}{\partial x_j}\left(\frac{\mu_t \partial ksgs}{\sigma_k \partial x_j}\right)$$

The model constants, Ck and C_ε, are determined dynamically (Kim & Menon, 1997) and σ_k is 1.0 in the above equations.

The wind speed profile shown in Figure 2 was collected from Dagnew et al. (2009) since the result of the current study required reliable data with whom it could be compared and come to a conclusive decision if the current study was accurate enough. In their 2009 study, Dagnew et al. presented wind tunnel test results along with those from Tong Ji University and CFD analysis using numerical models, specifically Large Eddy Simulation and K-epsilon. This study aimed to compare its results with those of Dagnew et al., as shown in Figure 5.

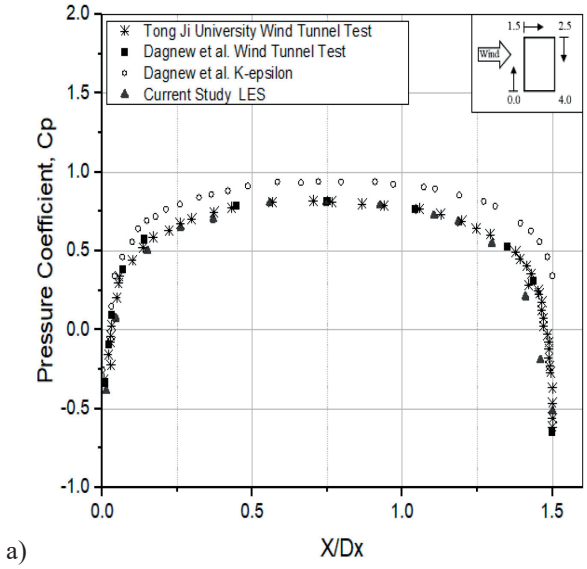

Fig. 5. Comparisons of wind pressure coefficient between current and previous studies on the CAARC building model (a) Windward (b) Leeward

The study found that in the windward face (X/Dx 0.0-1.5), the LES numerical model used in this study demonstrated greater accuracy than the K-epsilon model used by Dagnew et al., while both models agreed in the leeward face (X/Dx 2.5-4.0), and agreed with wind tunnels. The reference wind speed was 12.7 m/s. Wind pressure coefficients (Cp) were computed at 2/3H of the building on the leeward, sidewall, and windward sides for the inflow boundary conditions shown in Figures 3a and 3b.

3. WIND TUNNEL SETUP

The test portion of the wind tunnel is 27 feet long and 3.94 feet (width) by 2.80 feet in cross-section (height). The experimental flow is reproduced at a length scale of 1: 300 to replicate the features of an open rural area.

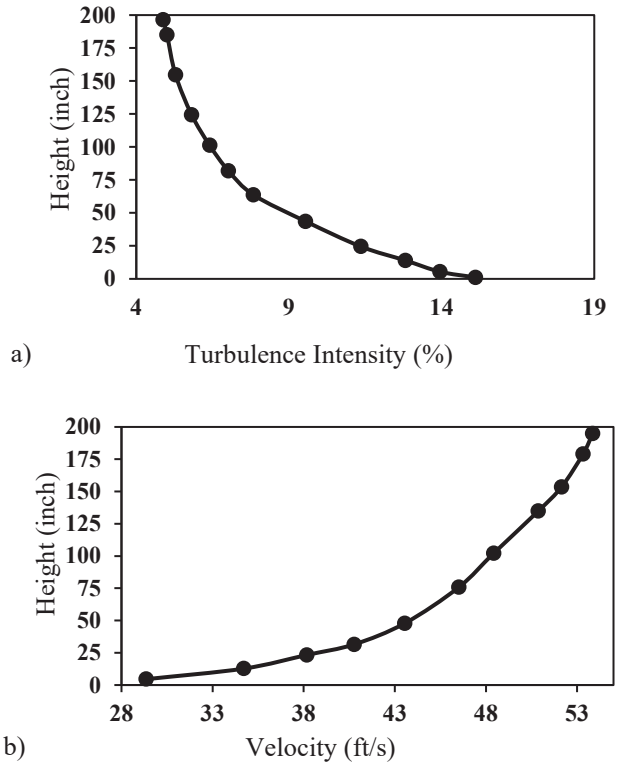

Fig. 6. Turbulence intensity (a) and Velocity profile (b)

Wind tunnel setup used in the study of (Amin & Ahuja, 2013) was followed with little adjustment for this study. The model is positioned 20 feet from the test section's upstream edge. In order to quantify the free stream velocity during experiments, a reference inlet and outlet tube is placed 20 inches above the wind tunnel floor and 11.5 feet away from the grid. Figures 6a and 6b, respectively, show the intensity of the turbulence and the non-dimensional mean

velocity. The reference wind speed used in this research has been kept constant at 40 ft/sec at the model's roof height. The power-law index (n) of the velocity profile within the tunnel is 0.162.

3.1. Information about models

The experiments utilized models made of translucent plastic, with a thickness of 0.25 inches. These models were created at a geometrical scale of 1:300, matching the scale used for the wind simulation. To ensure meaningful comparisons, the height and surface area of each model were kept constant at 15.5 square inches and 12 inches, respectively. To accurately measure pressure distribution on the building models' surfaces, approximately 175 pressure taps were installed at seven different height levels: 1, 3, 5, 7, 9, 10, and 11 inches from the floor. These pressure taps were strategically positioned near the faces of the models to capture fluctuations in high pressure along the edges. For further details on the classification and dimensions of the building models, refer to Table 1. Figure 7 illustrates the locations of the pressure taps around the perimeters of the building models, with measurements provided in inches.

Table 1. Features of the models

Model	Building Dimension (L x W x H)	Side Ratio	Computational Domain (X x Y x Z)	Blockage Ratio	
				0°	90°
M-1	4" x 4" x 12" [100 mm x 100 mm x 300 mm]	1.0	90" x 90" x 33" [2250 mm x 2250 mm x 825 mm]	1.61%	1.61%
M-2	3.2" x 5" x 12" [80 mm x 125 mm x 300 mm]	1.56		1.30%	2.02%
M-3	2.67" x 6" x 12" [75 mm x 150 mm x 300 mm]	2.25		1.08%	2.42%
M-4	2.24" x 7.15" x 12" [55 mm x 175 mm x 300 mm]	3.2		0.90%	2.89%

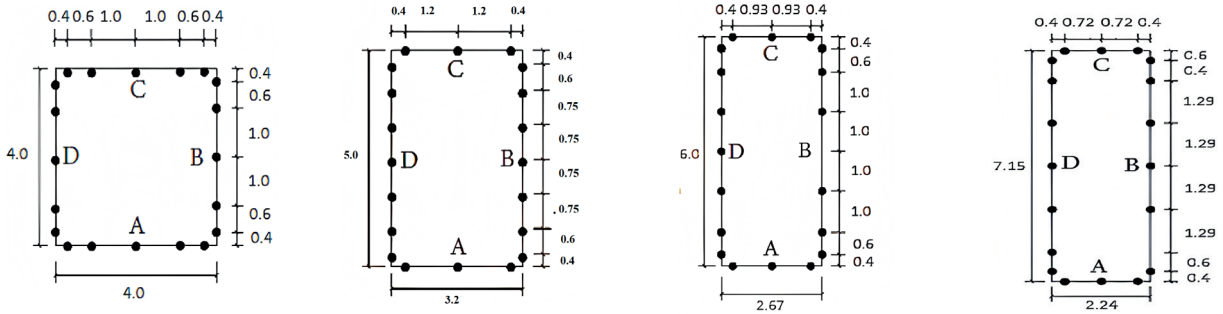

M-1 M-2 M-3 M-4

Fig. 7. The locations where pressure tapping was conducted along the perimeter and plan view of the models

4. RESULTS AND DISCUSSION

The varied wind pressure data were used to re-evaluate the pressure coefficients on every surface of building model throughout a range of wind angles of incidence from 0° to 90° at 15° intervals. The average (mean), root mean square (r.m.s.), and highest and lowest wind pressure coefficients were calculated during this reevaluation. The wind pressure coefficient contours of models M-1, M-2, M-3, and M-4 at a wind incidence angle of 0° are depicted in Figures 8, 10, 12, and 14 from the experimental while Figures 9, 11, 13, and 15 represent the wind pressure coefficient from the CFD analysis, respectively. These figures visually represent how the wind pressure varies across the surface of the models under study. By examining these contours, we can better understand the aerodynamic forces at play and how they affect the performance of the models.

The wind pressure coefficient distribution was relatively similar for models M1, M2, and M3 based on both experimental and CFD results. However, for model M4, the CFD results showed fewer wind pressure coefficient values, which can be observed in Figures 14 and 15.

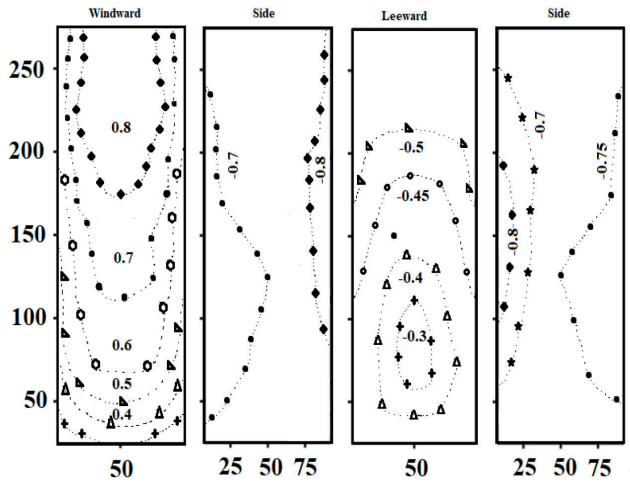

Fig. 8. Experimental wind pressure coefficient distribution for Model M-1

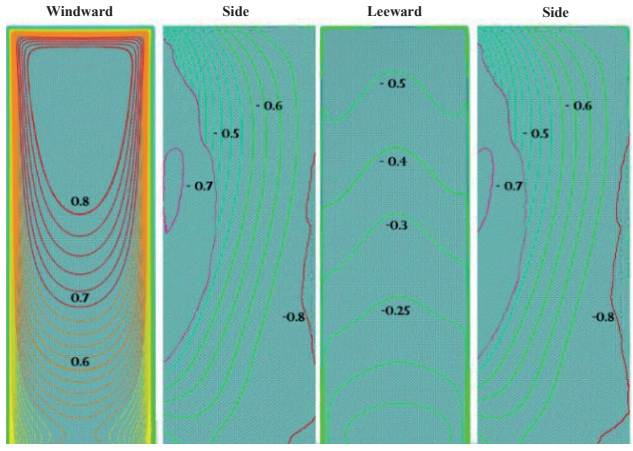

Fig. 9. CFD Analyzed wind pressure coefficient distribution for Model M-1

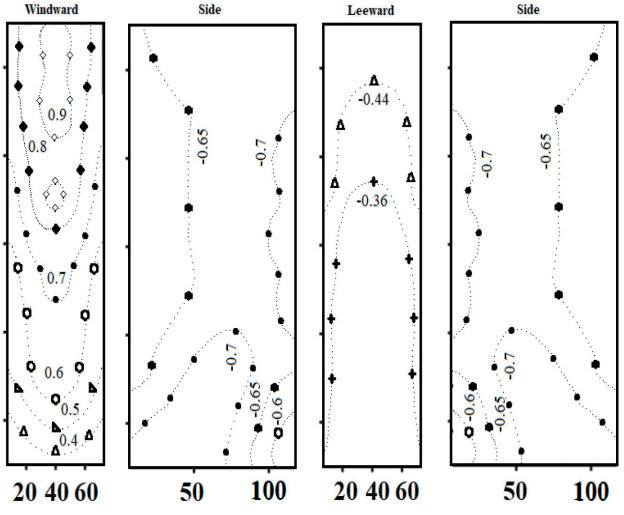

Fig. 10. Experimental wind pressure coefficient distribution for Model M-2

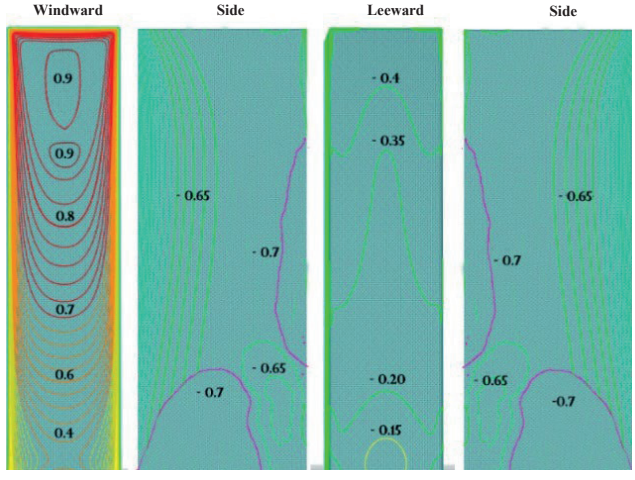

Fig. 11. CFD Analyzed wind pressure coefficient distribution for Model M-2

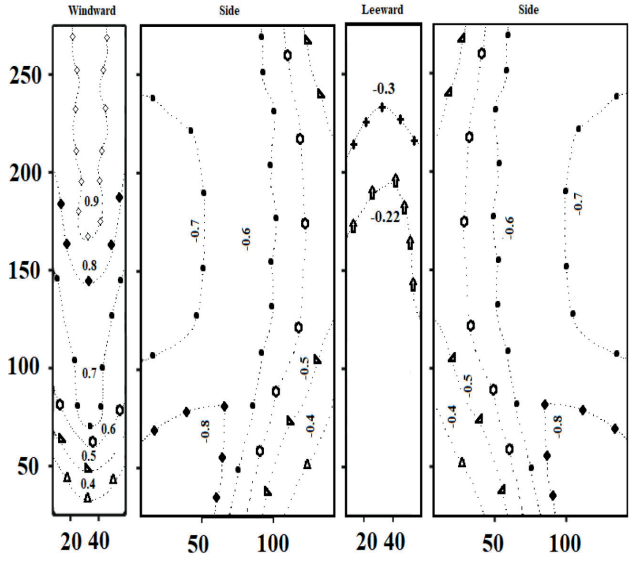

Fig. 12. Experimental wind pressure coefficient distribution for Model M-3

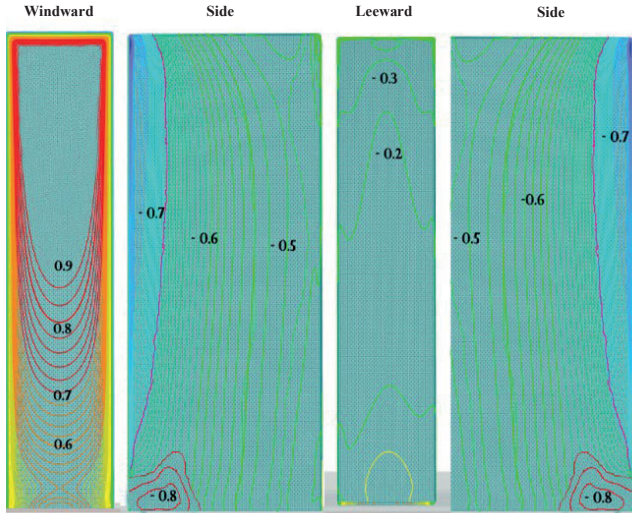

Fig. 13. CFD Analyzed wind pressure coefficient distribution for Model M-3

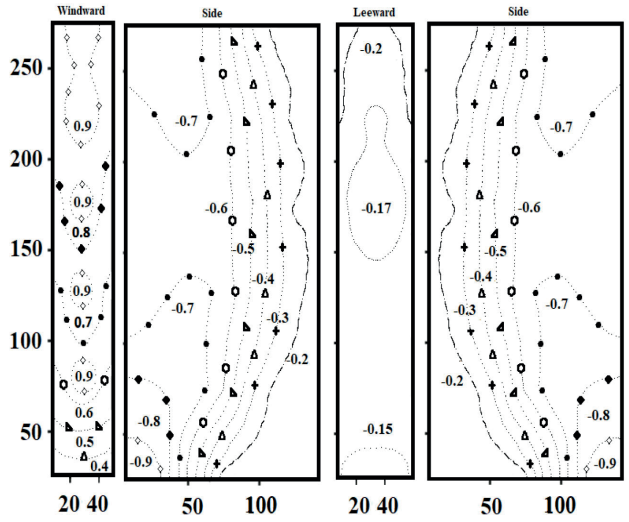

Fig. 14. Experimental wind pressure coefficient distribution for Model M-4

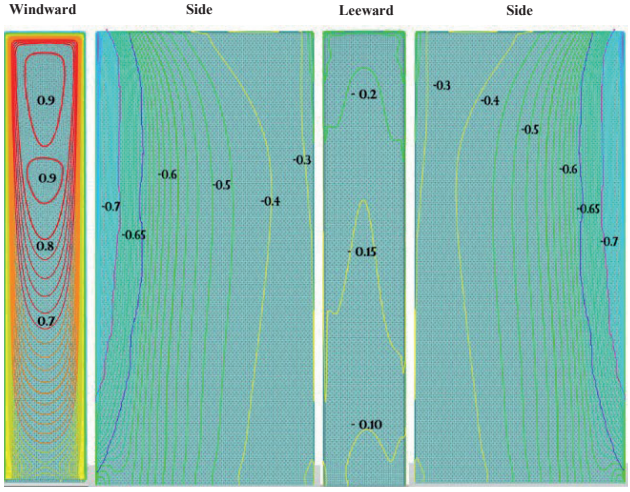

Fig. 15. CFD Analyzed wind pressure coefficient distribution for Model M-4

Experimental and CFD results have shown that the wind pressure distribution on models with different aspect ratios is significantly affected by both the height-to-width and height-to-length ratios. Upon analyzing the wind pressure coefficient values and distribution depicted in Figures 8 to 15, a few observations could be made. For instance, the positive pressure on model surfaces varied little (gentle), but higher positive wind pressures were observed on narrower windward sides. In contrast, larger windward side corresponded to more severe negative wind effects in the leeward side (Opposite side). Model M-3, and M-4 having a relatively narrower windward area compared with other models, showed a high positive pressure coefficient. On the other hand, M-1 having a relatively large windward surface showed higher negative pressure coefficient in the leeward side. The length of the side walls played little role in altering the positive wind pressure. Significant variations were observed in the pressure distribution on leeward surfaces, indicating intensified wind effects on leeward surfaces. Observing all the model's result it was found that the side wall peak wind pressure coefficient values remain almost same but the distribution varies with decrease in the windward width (surface). Furthermore, wider widths amplified both positive and negative effects in the vicinity of the models, while the negative effects diminished as the windward length of the models increased. The CFD analysis results agree with the remarks made by the experimental results.

Based on the results, it can be concluded that the size and shape of rectangular models have minimal impact on the distribution of pressure coefficients on the windward side. However, observations revealed that the root mean square and average pressure coefficients on the leeward side exhibit an increase up to a specific threshold, specifically at a side ratio of 0.6. Beyond this threshold, as the side ratio increases, both the mean and r.m.s. pressure coefficients decrease. This trend is visually depicted in Figure 16. These observations suggest the presence of an optimal side ratio for rectangular models in terms of wind resistance. Further research endeavors could delve into this concept and potentially contribute to the development of more efficient and effective designs for structures that require resilience in windy conditions.

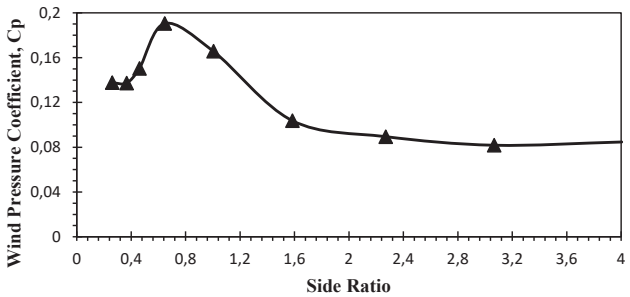

Fig. 16. The root mean square (R.M.S) wind pressure coefficient on the leeward side for various side ratios

Table 2 presents a comparison of wind pressure coefficients derived from experimental data and Computational Fluid Dynamic (CFD) analysis of building models at a wind incidence angle of 0°, alongside prominent wind standards and codes. Notably, all codes discussed in this study propose a pressure coefficient (Cp) of 0.8 for the

Table 2. Mean wind pressure coefficient comparison with CFD and different codes

Model	Side Ratio	Windward					Leeward					Side				
		Exp.	CFD	BNBC 2020	ASCE 7-05	AS/NZS 1170.2	Exp.	CFD	BNBC 2020	ASCE 7-05	AS/NZS 1170.2	Exp.	CFD	BNBC 2020	ASCE 7-05	AS/NZS 1170.2
M-1	1.00	0.74	0.76	0.8			-0,5	-0,5	-0.5	-0.5	-0.5	-0.69	-0.56	-0.7	-0.7	-0.65
M-2	1.56	0.74	0.77	0.8			-0,41	-0,41	-0.4	-0.4	-0.4	-0.66	-0.53	-0.7	-0.7	-0.65
M-3	2.25	0.75	0.78	0.8			-0,3	-0,28	-0.3	-0.3	-0.3	-0.62	-0.55	-0.7	-0.7	-0.65
M-4	3.20	0.75	0.79	0.8			-0,2	-0,18	-0.25	-0.25	-0.25	-0.59	-0.46	-0.7	-0.7	-0.65

windward side. Interestingly, the investigated models consistently exhibited mean Cp values lower than 0.8 on the windward face, indicating that the values recommended by the codes are reliable for rectangular-shaped buildings. Moreover, the mean Cp values obtained from both the experiment and CFD analysis for the leeward and side faces also matched or were lower than the values suggested by the codes. This suggests that despite significant fluctuations in Cp values along the side and leeward side, the engineering community can confidently rely on the values prescribed by the codes for rectangular-shaped buildings. Additionally, Table 2 provides insights into the influence of the side ratio on the pressure coefficient, a topic previously discussed.

5. CONCLUSION

The process of conducting wind pressure measurements on building models enables researchers to understand how side ratios and wind orientations affect wind pressure distribution and pressure coefficients on rectangular building models. According to the findings, the height-to-width and height-to-length ratios considerably impact the wind pressure distribution in models. When it comes to the positive pressure on model surfaces, smaller windward sides tend to have higher wind pressures than bigger windward sides, which are linked to more intense negative wind impacts. In contrast to previous models, Model M-3, and M-4 has a shorter windward area, but it nevertheless displays a high positive pressure coefficient over a sizable portion of the windward surface, suggesting stronger wind pressure at the windward face. On the other hand, the amount of positive wind pressure is not significantly affected by the length of the side walls. The wind's impacts are more pronounced on both sides, and leeward surfaces, and the pressure distribution on leeward surfaces exhibits significant changes.

The depth or side ratio of rectangular structures has no effect on the intensity or pattern of distribution of the amount of pressure coefficients on the windward side for the wind direction of 0°. The mean and r.m.s. pressure coefficients, however, increase in absolute value to an aspect ratio of 0.6 on the leeward side. Both the root mean square and average pressure coefficients on the side that faces leeward subsequently fall in absolute value as the side ratio continues to rise. When the aspect ratio exceeds 3.0, a consistent negative pressure coefficient is observed on the leeward side, suggesting that the object achieves a minimal width. This study highlights the necessity for more investigation into the connection between different planar forms and wind impacts. Future studies will explore additional planar shapes like ovals and crosses whereas this article only concentrates on rectangular shapes.

References

[1] ASCE:7-05, Minimum Design Loads for Buildings and other Structures, Structural Engineering Institute of the American Society of Civil Engineers, Reston, VA, USA, 2002.
[2] Amin J.A., Ahuja A.K. (2013): *Effects of side ratio on wind-induced pressure distribution on rectangular buildings*. Journal of Structures.
[3] Bangladesh National Building Code. (2020): Dhaka, Bangladesh: Housing and Building Research Institute.
[4] Baskaran A., Stathopoulos T. (1993): *Numerical computation of wind pressures on buildings*. Computers &structures, 46(6), 1029-1039; doi.org/10.1016/0045-7949(93)90089-V.
[5] Baskaran A., Stathopoulos T. (1989): *Computational evaluation of wind effects on buildings*. Building and Environment, 24(4), 325-333; doi.org/10.1016/0360-1323(89)90027-9.

[6] Blocken B. (2014): *50 years of computational wind engineering: past, present and future*. Journal of Wind Engineering and Industrial Aerodynamics, 129, 69-102; doi.org/10.1016/j.jweia.2014.03.008.
[7] Franke J., Hirsch C., Jensen A., Krüs H., Schatzmann M., Westbury P., Wright, N.G. (2004): *Recommendations on the use of CFD in wind engineering*, COST Action C14: Impact of Wind and Storm on City Life and Built Environment, von Karman Institute for Fluid Dynamics.
[8] Jóźwiak R., Kacprzyk J., Zurańsk J.A. (1995): *Wind tunnel investigations of interference effects on pressure distribution on a building*. Journal of wind engineering and industrial aerodynamics, 57(2-3), 159-166; doi.org/10.1016/0167-6105(95)00004-B.
[9] Kareem A. (1990): *Measurements of pressure and force fields on building models in simulated atmospheric flows*. Journal of Wind Engineering and Industrial Aerodynamics, 36, 589-599; doi.org/10.1016/0167-6105(90)90341-9.
[10] Kareem A., Cermak J.E. (1984): *Pressure fluctuations on a square building model in boundary-layer flows*. Journal of Wind Engineering and Industrial Aerodynamics, 16(1), 17-41; doi.org/10.1016/0167-6105(84)90047-3.
[11] Kwon D.K., Kareem A. (2013): *Comparative study of major international wind codes and standards for wind effects on tall buildings*. Engineering Structures, 51, 23-35; doi.org/10.1016/j.engstruct.2013.01.008.
[12] Kim W.W., Menon S. (1997): *Application of the localized dynamic subgrid-scale model to turbulent wall-bounded flows*. Technical report AIAA-97-0210. Reno (NV): American Institute of Aeronautics and Astronautics, 35th Aerospace Sciences Meeting.
[13] Lee B.E. (1975): *The effect of turbulence on the surface pressure field of a square prism*. Journal of Fluid Mechanics, 69(2), 263-282; doi.org/10.1017/S0022112075001437.
[14] Miyata T., Miyazaki M. (1980): *Turbulence effects on aerodynamic response of rectangular bluff cylinders*. In Wind Engineering (pp. 631-642). Pergamon.
[15] Murakami S., Mochida A., Hibi K. (1987): *Three-dimensional numerical simulation of air flow around a cubic model by means of large eddy simulation*. Journal of Wind Engineering and Industrial Aerodynamics, 25(3), 291-305; doi.org/10.1016/0167-6105(87)90023-7.
[16] Murakami S., Mochida A. (1988): *3-D numerical simulation of airflow around a cubic model by means of the k-ϵ model*. Journal of Wind Engineering and Industrial Aerodynamics, 31(2-3), 283-303.
[17] Standards Australia. (2011). AS/NZS 1170.2 Structural Design Actions, Part 2 Wind Actions; doi.org/10.1016/0167-6105(88)90009-8.
[18] Saathoff P.J., Melbourne W.H. (1989): *The generation of peak pressures in separated/reattaching flows*. Journal of Wind Engineering and Industrial Aerodynamics, 32(1-2), 121-134; doi.org/10.1016/0167-6105(89)90023-8.
[19] Stathopoulos T., Baskaran B.A. (1996): *Computer simulation of wind environmental conditions around buildings*. Engineering structures, 18(11), 876-885; doi.org/10.1016/0141-0296(95)00155-7.
[20] Vickery B.J. (1966): *Fluctuating lift and drag on a long cylinder of square cross-section in a smooth and in a turbulent stream*. Journal of Fluid Mechanics, 25(3), 481-494; doi.org/10.1017/S002211206600020X.